

Mesoscopic conductance fluctuations in graphene

D. W. Horsell,¹ A. K. Savchenko,¹ F. V. Tikhonenko,¹ K. Kechedzhi,² I. V. Lerner,³ and V. I. Fal'ko²

¹*School of Physics, University of Exeter, Stocker Road, Exeter, EX4 4QL, UK*

²*Department of Physics, Lancaster University, Lancaster, LA1 4YB, UK*

³*School of Physics and Astronomy, University of Birmingham, Birmingham B15 2TT, UK*

We study fluctuations of the conductance of micron-sized graphene devices as a function of the Fermi energy and magnetic field. The fluctuations are studied in combination with analysis of weak localization which is determined by the same scattering mechanisms. It is shown that the variance of conductance fluctuations depends not only on inelastic scattering that controls dephasing but also on elastic scattering. In particular, contrary to its effect on weak localization, strong intervalley scattering suppresses conductance fluctuations in graphene. The correlation energy, however, is independent of the details of elastic scattering and can be used to determine the electron temperature of graphene structures.

PACS numbers: 73.23.-b, 72.15.Rn, 73.43.Qt, 81.05.Uw

INTRODUCTION

Fluctuations of the conductance of electron systems have been studied for many years in metals and electron gases formed in semiconductors [1]. They originate from the interference between phase-coherent electron paths that cross the system, and in diffusive, phase-coherent systems the conductance fluctuations are universal (UCF): their average amplitude of the order of e^2/h is independent of the mean conductance [2]. Another consequence of quantum coherence in diffusive systems is a weak localization (WL) correction to the conductance. It was shown recently that WL in a new two-dimensional system, graphene [3], is unusual in that it depends not only on inelastic but also elastic scattering of chiral carriers, both within and between the two graphene valleys [4, 5].

As quantum interference lies at the origin of both UCF and WL, it is important to understand if manifestation of UCF in graphene is also different from that in conventional two-dimensional systems. In our earlier studies of WL in monolayer and bilayer graphene [5, 6] we have established that quantum interference of carriers within one valley is suppressed, but the presence of significant intervalley scattering makes it clearly detectable in the magnetoconductance. Here we perform the first analysis of conductance fluctuations in graphene, both in the metallic and electro-neutrality (Dirac) regions, which are complemented by WL studies. Using recent theories of UCF in graphene [7, 8, 9], we show that, similar to WL, the amplitude of the fluctuations can be strongly affected by the intensity of elastic scattering, so that it can be larger than in conventional 2D metals. In graphene flakes, however, significant intervalley scattering reduces it to a value close to that in one-valley 2D systems with non-chiral carriers. In order to detect the unusual properties of UCF in graphene with a significant (up to four times) increase of the variance, one has to fabricate samples with no intravalley suppression of interference as well

as weak intervalley scattering.

We also examine the effect of elastic scattering in graphene on the autocorrelation function of the fluctuations as a function of the Fermi energy, and show that under usual experimental conditions the correlation energy is insensitive to the specifics of scattering and can be used as a direct measure of the electron temperature. Methods to determine the true electron temperature become important in graphene-based devices where phonons are poorly coupled to the environment, so that with commonly used currents the overheating of electrons is highly likely. The classical conductivity has a very weak temperature dependence [10] and therefore is not suitable for this purpose. Both the WL and the variance of UCF have strong temperature dependences [5, 6], but the magnitudes of these effects depend on the details of inelastic and elastic scattering and so do not readily allow for the extraction of the temperature from them. We show here that analysing the width of the correlation function does unambiguously yield the electron temperature in graphene, as well as in any mesoscopic diffusive conductor.

THEORY

The variance of the conductance fluctuations in graphene is determined by the standard set of the perturbation theory diagrams in $\hbar/(p_F\ell) \ll 1$ (ℓ is the electron mean free path) shown in Fig. 1. Structurally, they coincide with the diagrams describing mesoscopic fluctuations in usual conductors [11] but the Hikami boxes are different [7, 8, 12] because of the linear energy spectrum, carrier chirality and valley degeneracy in graphene. In the low-temperature limit, $L_T \gg L_\varphi$, where $L_T = (\hbar D/k_B T)^{1/2}$ is the thermal diffusion length, $L_\varphi = (D\tau_\varphi)^{1/2}$, (D is the diffusion coefficient and τ_φ is the phase-breaking time), the variance of conductance

fluctuations becomes [7, 8]

$$\langle \delta G^2 \rangle \equiv \mathcal{F}(0) = \frac{12}{\beta} g_s^2 \mathcal{R}(L, W, L_\varphi, L_i, L_*), \quad (1)$$

where G is the conductance in units of e^2/h , $\delta G = G - \langle G \rangle$, W and L are, respectively, the sample width and length, g_s is the spin degeneracy, and the time-reversal symmetry parameter $\beta = 1$ for $B \ll B_0 = (\hbar/e)/L_\varphi^2$ and $\beta = 2$ for $B \gg B_0$. The function $\mathcal{R}(L, W, L_\varphi, L_i, L_*)$ is given by

$$\begin{aligned} \mathcal{R} = & \sum_{n=1, m=0}^{\infty} \{ \eta_{nm}^{-2} + \\ & (\eta_{nm} + 2(L/L_i)^2)^{-2} + \\ & 2(\eta_{nm} + ((L/L_i)^2 + (L/L_*)^2))^{-2} \} \\ & = \mathcal{R}_1 + \mathcal{R}_2 + 2\mathcal{R}_3, \end{aligned} \quad (2)$$

where $\eta_{nm} = \pi^2 n^2 + (L/W)^2 \pi^2 m^2 + (L/L_\varphi)^2$, $L_i = (D\tau_i)^{1/2}$ is the intervalley scattering length determined by the scattering rate τ_i^{-1} , and $L_* = (D/(\tau_w^{-1} + \tau_z^{-1}))^{1/2}$ stands for the intravalley scattering length determined by both the trigonal-warping scattering rate τ_w^{-1} and the scattering rate τ_z^{-1} due to sublattice asymmetric potentials [4].

In the case of $L_\varphi \gg L$ the conductance variance given by Eqs. 1 and 2 is independent of the dephasing length and can be represented as $\mathcal{R} = \alpha \mathcal{R}_1$, $4 \geq \alpha \geq 1$. The coefficient α is sensitive to the strength of intervalley and intravalley scattering in a particular graphene sample. Namely, $\alpha = 4$ if $L_i, L_* \gg L$; $\alpha = 1$ for $L \gg L_i$; and $\alpha \approx 2$ for $L_i > L > L_*$. Therefore, the variance of conductance fluctuations in graphene is different from that in a conventional metal [2], in which case $\mathcal{R} = \mathcal{R}_1$ in Eq. 2 and the variance is insensitive to the microscopic details of disorder. In the case of a long and narrow graphene sample, strong intervalley scattering at the edges ($L \gg L_i$) results in $\alpha = 1$ and $\mathcal{R}_1 = \zeta(4)/\pi^4$, leading to $\langle \delta G^2 \rangle = (2/\beta)g_s^2/15$, which coincides with the usual result for quasi-1D disordered wires.

At finite temperatures, the autocorrelation function of conductance fluctuations, $F(\Delta)$, is given by a convolution of the ensemble-averaged correlator, $\mathcal{F}(\varepsilon) \equiv \langle \delta G(E) \delta G(E + \varepsilon) \rangle$, and the thermal broadening factor

$$K(\varepsilon, \Delta) = \int dE f'(E, \varepsilon_F) f'(E + \varepsilon, \varepsilon_F + \Delta),$$

where $f'(E, \varepsilon_F) = -1/(4k_B T_e) \cosh^{-2}[(E - \varepsilon_F)/(2k_B T_e)]$ is the energy derivative of the Fermi-Dirac distribution function (T_e is the electron temperature). Thus

$$\begin{aligned} F(\Delta) & \equiv \langle \langle \delta G(\varepsilon_F) \delta G(\varepsilon_F + \Delta) \rangle \rangle \\ & = \int d\varepsilon K(\varepsilon, \Delta) \mathcal{F}(\varepsilon). \end{aligned} \quad (3)$$

Here the brackets $\langle \langle \dots \rangle \rangle$ stand for both the ensemble and thermal averaging and

$$\mathcal{F}(\varepsilon) = 4g_s^2 \sum_{n,m} \sum_{l=1,2,3,4} \left(|\mathcal{D}_{nm}^l|^2 + \frac{1}{2} \text{Re} [\mathcal{D}_{nm}^l]^2 \right), \quad (4)$$

$$\mathcal{D}_{nm}^1 \equiv \left(-\frac{i}{\hbar} \varepsilon \tau_D + \eta_{nm} \right)^{-1}, \quad (5)$$

$$\mathcal{D}_{nm}^2 \equiv \left(-\frac{i}{\hbar} \varepsilon \tau_D + \eta_{nm} + 2(L/L_i)^2 \right)^{-1}, \quad (6)$$

$$\mathcal{D}_{nm}^{3,4} \equiv \left(-\frac{i}{\hbar} \varepsilon \tau_D + \eta_{nm} + (L/L_i)^2 + (L/L_*)^2 \right)^{-1}, \quad (7)$$

where $\tau_D \equiv L^2/D$.

The variance of the conductance in graphene and the correlator $\mathcal{F}(\varepsilon)$ given by Eqs. 4-7 are sensitive to the microscopic details of disorder in a particular sample. However, in the normalized autocorrelation function $F_n \equiv F(\Delta)/F(0)$ these details do not manifest themselves under usual experimental conditions.

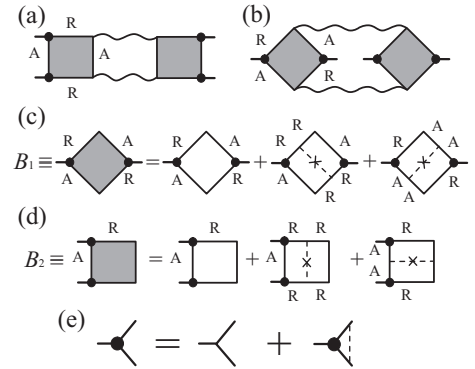


FIG. 1: (a),(b) The diagrams which contribute to the main order in the diagrammatic expansion of the conductivity-conductivity correlation function. The solid lines are the impurity averaged retarded or advanced Green functions, the short wavy tails are the current vertices and the long wavy lines the diffusion ladders. (c),(d) Hikami boxes of two types and additional diagrams which determine renormalization in the main order in $1/k_F l \ll 1$, where the dashed lines correspond to the disorder potential. (e) Diagrammatic equation for renormalized current vertex.

To show this, let us first consider a narrow wire, $W \ll \min(L_\varphi, L)$, with strong intervalley scattering at the boundaries. Then the part of the correlator \mathcal{F} which contributes to F_n can be written exclusively via the ‘valley-singlet’ diffusion propagators \mathcal{D}_{nm}^1 . The sum over m in Eq. 4 in this case is dominated by the $m = 0$ term. (Note that we have taken into account only the diffusion modes and neglected the Cooperons, which corresponds to the regime of suppressed WL by magnetic field.) We obtain an asymptotic expression for $F_n(\Delta)$ assuming $L \gg L_\varphi$ keeping only the term with $m = 0$ and

performing the summation over n :

$$\mathcal{F}(\varepsilon) = 4g_s^2 \left(\frac{1}{2\sqrt{2}} \left(\frac{L_\varphi}{L_x} \right)^3 \frac{3t^2 + t + 2}{t^3\sqrt{t+1}} - \left(\frac{L_\varphi}{L_x} \right)^4 \frac{t^2 + 2}{t^4} \right), \quad (8)$$

where $t \equiv \sqrt{(\varepsilon\tau_\varphi/\hbar)^2 + 1}$. This function is sharply peaked, with a maximum at $\varepsilon = 0$ and width \hbar/τ_φ . In contrast, the thermal broadening factor $K(\varepsilon, \Delta)$ has a broad peak at $\varepsilon = \Delta$ of width $\sim k_B T_e \gg \hbar/\tau_\varphi$. Convolution of these functions results in a normalized correlation function that is independent of the microscopic details contained in $\mathcal{F}(\varepsilon)$:

$$F_n(\Delta) = \frac{K(0, \Delta)}{K(0, 0)} = \frac{3(\theta \coth \theta - 1)}{\sinh^2 \theta}, \quad \theta \equiv \frac{\Delta}{2k_B T_e}. \quad (9)$$

The width of this one-parameter function, determined from $F_n(\theta_c) = 0.5$, is $\theta_c = 1.36$, which results in

$$\Delta_c \approx 2.7k_B T_e. \quad (10)$$

This result remains valid under the condition $L_T, L_y \ll \min(L_\varphi, L_x)$ for any $L_\varphi \lesssim L_x$, and allowing for all the diffusion modes in Eqs. 5-7 in graphene or, indeed, in any other mesoscopic disordered conductor. This result was tested numerically in [9]. There, the values of Δ_c were found to lie within a narrow interval, $2.7 \leq \Delta_c/k_B T_e \leq 2.9$, within 10% of the asymptotic value 2.7 of Eq. 10. Good agreement with this value (within 25%) was also found when 2D samples were considered.

EXPERIMENT

The samples studied experimentally in this work are monolayer graphene flakes created by mechanical exfoliation on a n^+ Si substrate covered by 300 nm of SiO_2 . In addition to monolayer graphene flakes, we have also studied a bilayer sample (Bi: $L = 1.5 \mu\text{m}$, $W = 1.8 \mu\text{m}$, see [6]), to examine the generality of the method of determining the electron temperature. (The number of layers in the studied structures has been established from the analysis of the quantum Hall effect [5, 6].) The manifestation of WL effects in monolayer and bilayer graphene can be very different, but the correlation properties of conductance fluctuations as a function of the Fermi energy are expected to be universal.

The ac current driven through the sample was 1 nA to avoid overheating (determined by measuring the effect of increasing the current on the mesoscopic fluctuations). The Fermi energy, ε_F , was controlled by a gate voltage, V_g , applied between the substrate and the flake (in our monolayers, $\varepsilon_F = \hbar v_F \sqrt{\pi V_g C}/e$, where C is the capacitance per unit area between the gate electrode and graphene). The conductance of all samples is shown as a function of Fermi energy in Fig. 2. The dephasing rate

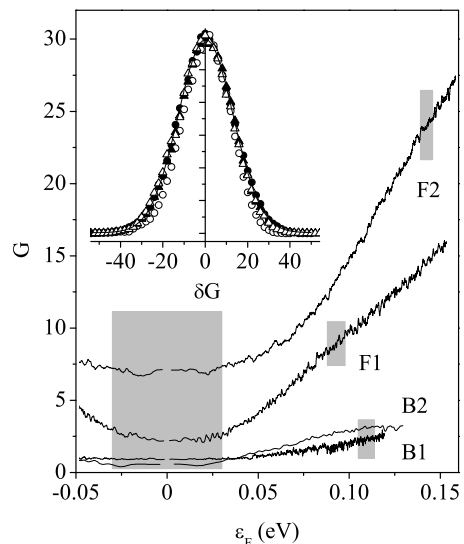


FIG. 2: Dimensionless conductance of the graphene samples as a function of the Fermi energy at $T = 0.25$ K. (For B2 the hole region is studied so the scale has been reversed to compare with other samples.) The shaded regions show the energy range used in the analysis. The inset shows the distribution function of δG for sample F2 averaged over ~ 14000 ‘realisations’ (filled symbols are for high density, open symbols for the Dirac region).

Sample	L	W	$L_\varphi^{0.25\text{ K}}$	$L_\varphi^{4\text{ K}}$	L_i	L_*	ℓ	n
F1	4.1	1.8	1.5	0.7	0.4	0.06	0.07	1.4
F2	3.8	1.8	3.8	1.7	0.5	0.1	0.1	0.7

TABLE I: Lengthscales (in microns) of samples F1 and F2 at high carrier density. The values of the dephasing length, L_φ have been determined from analysis of the weak localization. Shown here are values at $T = 0.25$ K ($L_\varphi^{0.25\text{ K}}$) and 4 K ($L_\varphi^{4\text{ K}}$). ℓ is the mean free path and n is the carrier density in 10^{12} cm^{-2} .

was determined from a fit of the magnetic field dependence of the sample conductance to the theory of weak localization in graphene [4, 5]. (Indeed, in order to analyse the UCF properly the values of not only L_φ but also L_i and L_* need to first be determined and this can only be done in combination with analysis of the WL.) The sample parameters are given in [9] and extra details of samples F1 and F2 are given in Table I. Samples B1 and B2 are quasi-1D samples with width $W = 0.3 \mu\text{m}$ and length $L = 3.7$ and $2.0 \mu\text{m}$, respectively.

Fluctuations of the conductance occur as a function of both the Fermi energy and perpendicular magnetic field. The fingerprint of the fluctuations is robust and temperature dependent over the whole experimental range of 0.26 to 20 K. For a particular range of energies and fields the autocorrelation function $F(\Delta)$ of the fingerprints can be analysed to determine the variance $F(0)$ and the correlation energy Δ_c from $F(\Delta_c) = F(0)/2$. The V_g range

was chosen to incorporate a sufficient number (~ 100) of fluctuations without significantly changing the average value of the conductance. In our experiments this limits the range of temperatures to $T < 10$ K. To increase the number of fluctuations (sample ‘realisations’) the measurements were performed at several (10 – 20) values of magnetic field in the range $B \gg B_0$.

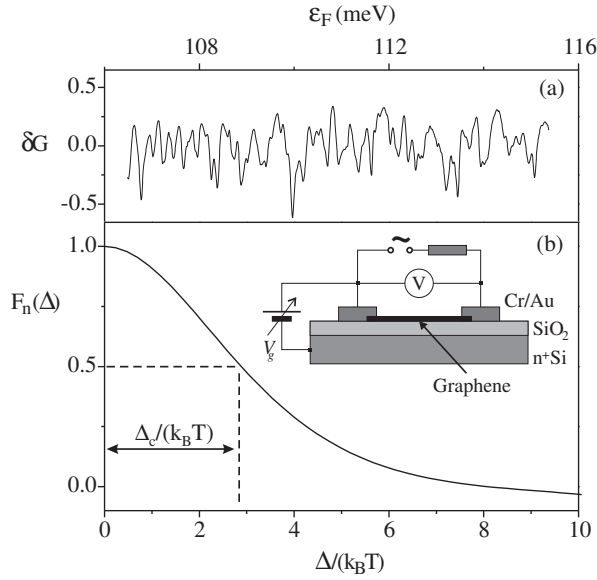


FIG. 3: (a) Typical fingerprint of δG (normalized by e^2/h) for sample B1 at $T = 0.25$ K and $B = 90$ mT as a function of Fermi energy. (b) Normalized correlation function for sample B1. The inset shows the circuit used in the experiment and construction of the graphene sample.

Figure 3(a) shows a typical fingerprint of conductance fluctuations (with average background, $\langle G \rangle$, removed) in sample B1 as a function of the Fermi energy in a magnetic field of 90 mT. In Fig. 3(b) the (normalized) autocorrelation function of the fingerprint in (a) is shown. In the inset of the figure the circuit used in the measurements is shown.

The random nature of the fluctuations is demonstrated for sample F2 in the inset of Fig. 2 where the distribution of the conductance fluctuations is seen to have a Gaussian shape typical of UCF [13]. (It is also seen that for this sample the magnitude of the fluctuations is very similar at high carrier density and in the Dirac region.) Figure 4 shows the variance of samples F1 and F2 at high carrier density. One can see immediately that the variance is temperature dependent over the whole range of temperatures down to 0.25 K. In the WL experiment, however, it was found that the magnitude of the quantum correction determined by L_φ saturates at low temperatures [5] (when $L_\varphi \sim L$). This highlights the importance of the lengthscale L_T for the amplitude of UCF in 2D, when $L_T < L_\varphi$ [15].

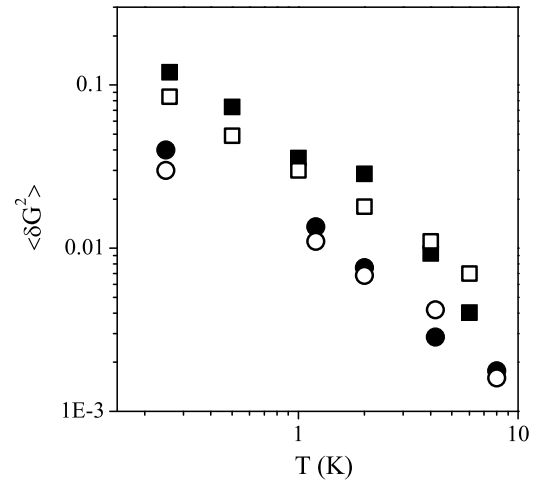


FIG. 4: The variance of the conductance fluctuations of sample F1 (circles) with those of sample F2 (squares). Solid symbols correspond to the experimental results while open ones represent theoretical values calculated using Eqs. 3-7 for $F(0)$.

ANALYSIS AND DISCUSSION

Using the values of L_φ , L_i and L_* determined from weak localization measurements in Eq. 3 we are able to calculate numerically the theoretical values of the variance for our samples. For F1 and F2, $L_\varphi \sim L > L_i \gg L_*$. One can see from Eq. 2 that the last two terms in \mathcal{R} are suppressed by the strong elastic scattering and therefore $\alpha \sim 1$. The good agreement between theory and experiment, Fig. 4, shows that L_φ calculated from WL and UCF is the same quantity, as predicted in [14], and also that unlike its effect in WL intervalley scattering acts to suppress the conductance fluctuations. In [5] it was shown that there is strong intravalley suppression of quantum interference in graphene deposited on silica, hence the four-fold increase of conductance fluctuations (Theory section) will not be seen. In addition, due to intervalley scattering at the sample edges the intervalley diffusion length L_i has an upper limit of the sample width. Therefore in narrow graphene samples it is difficult to achieve conditions where $\alpha > 1$, and as a result the amplitude of fluctuations is similar to that observed in a usual diffusive metal. We found previously [16] that the fluctuations in bilayer sample Bi can also be interpreted using a standard UCF model. This shows a dramatic contrast with WL where in the presence of intervalley scattering the shape of the magnetoconductance curve shows strong dependence on small variations in the elastic scattering.

The values of the correlation energy extracted from the correlation functions are shown in Fig. 5(a). It can be seen that the correlation energy increases linearly with increasing bath temperature. Equation 10 is plotted in Fig. 5 as a solid line. There is agreement between the

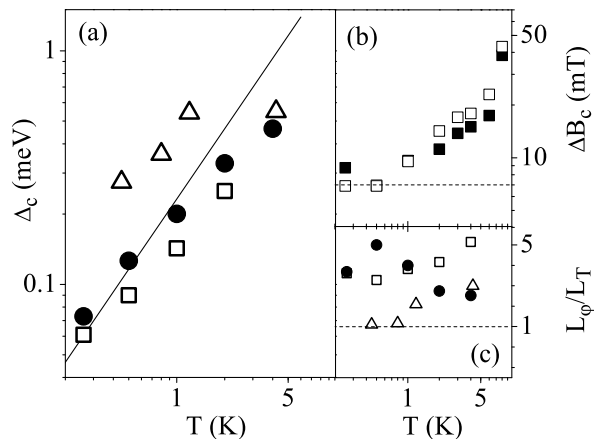


FIG. 5: (a) Experimental value of the correlation function width Δ_c for various bath temperatures extracted from the UCF in four graphene-based devices at high carrier density (F2: open squares, B1: filled circles, Bi: open triangles). The solid line corresponds to Eq. 10. (b) Correlation magnetic field of sample B2. Filled squares are experimental results and open squares are $\Delta B_c = (h/e)/WL_\phi$. The dashed horizontal line shows $\Delta B_c = (h/e)/WL$. (c) Ratio L_ϕ/L_T for high carrier densities in samples F2, B1 and Bi.

theory and experiment for all the samples. This includes the bilayer sample (open triangles in figure), which contrasts with the significant difference between monolayer and bilayer samples in the manifestation of weak localization [6, 17, 18]. This also indicates general applicability of the developed model to all diffusive systems. The criterion of the applicability of the theoretical result in Eq. 10, $L_\phi/L_T > 1$, is seen to be satisfied in the studied samples, Fig. 5(c).

We want to note that the results of our experiments on graphene show some general properties of UCF [2]. Increasing magnetic field above B_0 has shown the conventional decrease of the variance by a factor of two. Also, the correlation magnetic field has been seen to be related to $L_\phi(T)$ in the usual way. Shown in Fig. 5(b) is the correlation field for sample B2 as a function of temperature. For this sample $L_\phi > W$, so the expected dependence of the correlation field is $\Delta B_c(T) \approx (h/e)/WL_\phi(T)$ [1]. This is plotted as open squares in the figure and clear agreement is seen with experiment, including the saturation of ΔB_c that occurs at low temperatures when the dephasing length approaches the sample length.

Finally we discuss the results of our measurements in the Dirac region where the applicability of the developed analytical theory of UCF is not obvious, although the conductivity of our samples satisfies the commonly used criterion for the diffusion theory, $\langle G \rangle L/W \gg 1$. (We have also shown previously [5] that the diffusive theory of weak localization describes well the magnetoconductance in the Dirac region.) Numerical investigation of the conductance fluctuations in graphene (from sample

to sample) [19] have shown that their amplitude is considerably stronger than in conventional metals. At the same time experiments on few-layer samples [20] has claimed that conductance fluctuations (as a function of the carrier density) are suppressed near the charge neutrality point.

In our experiments we consider a region of carrier densities around the Dirac point, $-30 < \varepsilon_F < 30$ meV. Firstly, we do not observe an increase of the amplitude of conductance fluctuations in the Dirac region compared with that in the high-density regions. In samples F1 and F2 the variance in the Dirac region is very close to that in high-density regions, while in narrow samples B1 and B2 it is several times smaller. Secondly, it can be seen from Fig. 6 that the correlation energy deviates from the ‘high temperature’ limit at low temperatures. This can be attributed to the fact that for all samples the high-temperature condition is now destroyed because of a decrease of the dephasing length by $> 30\%$ that occurs when moving from high to low carrier density, Fig. 6(inset). (This decrease of the low-temperature dephasing length in the Dirac region was obtained from the analysis of WL in both monolayer and bilayer graphene samples [5, 6].)

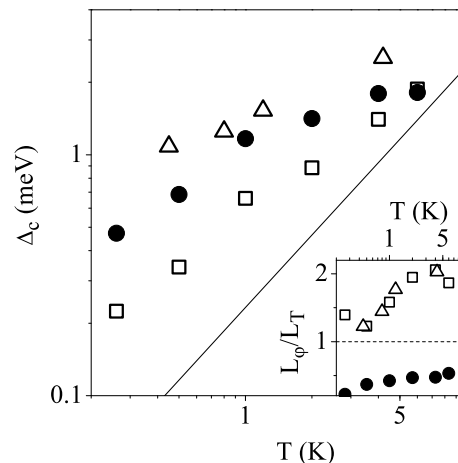


FIG. 6: Δ_c as a function of bath temperature at carrier density close to the Dirac point (F2: open squares, B1: filled circles, Bi: open triangles). The solid line corresponds to Eq. 10. Inset: Ratio L_ϕ/L_T at low carrier density in samples F2, B1 and Bi.

CONCLUSION

In conclusion, in combined studies of conductance fluctuations and weak localization in monolayer and bilayer flakes we have demonstrated that the variance of universal conductance fluctuations in graphene is strongly affected by elastic scattering, in particular intervalley scattering. However, the correlation energy of the fluctu-

ations as a function of the Fermi energy is insensitive to these scattering mechanisms under common experimental conditions. Analysis of this correlation energy allows direct measurement of the electron temperature in graphene structures. We have also discussed the evolution of the variance and the correlation energy of the conductance fluctuations from the region of high carrier density to the region close to the point of electro-neutrality.

We gratefully acknowledge financial support from the EPSRC (EP/D031109), the Lancaster–EPSRC Portfolio Partnership (EP/C511743) and ESF FoNE CRP ‘SpiCo’. We also thank R. V. Gorbachev for graphene sample preparation and P. R. Wilkins for technical support.

-
- [1] C. W. J. Beenakker, and H. Van Houten, *Solid State Physics* **44**, 1 (edt. by H. Ehrenreich and D. Turnbull, Academic Press Inc., San Diego, 1991).
 - [2] P. A. Lee and A. D. Stone, *Phys. Rev. Lett.* **55**, 1622 (1985); B. L. Altshuler, *JETP Lett.* **41**, 648 (1985).
 - [3] K. S. Novoselov, A. K. Geim, S. V. Morozov, D. Jiang, Y. Zhang, S. V. Dubonos, I. V. Grigorieva, and A. A. Firsov, *Science* **306**, 666 (2004).
 - [4] E. McCann, K. Kechedzhi, V. I. Fal’ko, H. Suzuura, T. Ando, and B. L. Altshuler, *Phys. Rev. Lett.* **97**, 146805 (2006).
 - [5] F. V. Tikhonenko, D. W. Horsell, R. V. Gorbachev, and A. K. Savchenko, *Phys. Rev. Lett.* **100**, 056802 (2008).
 - [6] R. V. Gorbachev, F. V. Tikhonenko, A. S. Mayorov, D. W. Horsell and A. K. Savchenko, *Phys. Rev. Lett.* **98**, 176805 (2007).
 - [7] K. Kechedzhi, O. Kashuba, and V. I. Falko, *Phys. Rev. B* **77**, 193403 (2008).
 - [8] M. Yu. Kharitonov and K. B. Efetov, *Phys. Rev. B* **78**, 033404 (2008).
 - [9] K. Kechedzhi, D. W. Horsell, F. V. Tikhonenko, A. K. Savchenko, R. V. Gorbachev, I. V. Lerner and V. I. Fal’ko, arXiv:0808.3211, to be published in *Phys. Rev. Lett.*
 - [10] S. V. Morozov, K. S. Novoselov, M. I. Katsnelson, F. Schedin, D. C. Elias, J. A. Jaszczak and A. K. Geim, *Phys. Rev. Lett.* **100**, 016602 (2008).
 - [11] B. L. Altshuler and D. E. Khmelnitskii, *JETP Lett.* **42**, 359 (1985).
 - [12] J. Wurm, A. Rycerz, I. Adagideli, M. Wimmer, K. Richter and H.U. Baranger, arXiv:0808.1008.
 - [13] B. L. Altshuler, V. E. Kravtsov, and I. V. Lerner, *JETP Lett.* **43**, 441 (1986); O. Tsypliyatyev, I. L. Aleiner, V. I. Fal’ko, and I. V. Lerner, *Phys. Rev. B* **68**, 121301(R) (2003).
 - [14] I. L. Aleiner and Ya. M. Blanter, *Phys. Rev. B* **65**, 115317 (2002).
 - [15] P. A. Lee, A. D. Stone, and H. Fukuyama, *Phys. Rev. B* **35**, 1039 (1987).
 - [16] R. V. Gorbachev, F. V. Tikhonenko, A. S. Mayorov, D. W. Horsell and A. K. Savchenko, *Physica E* **40**, 1360 (2008).
 - [17] K. Kechedzhi, V. I. Falko, E. McCann and B. L. Altshuler, *Phys. Rev. Lett.* **98** 176806 (2007).
 - [18] D. W. Horsell, F. V. Tikhonenko, R. V. Gorbachev and A. K. Savchenko, *Phil. Trans. R. Soc. A* **366**, 245 (2008).
 - [19] A. Rycerz, J. Tworzydło, and C.W.J. Beenakker, *Europhys.Lett.* **79**, 57003 (2007).
 - [20] N. E. Staley, C. Puls, and Y. Liu, *Phys. Rev. B* **77**, 155429 (2008).